Proceedings of ICEGEE 2026 Symposium: AI-Based Medicine and Biological Data Analysis
DOI: 10.54254/2753-8818/2026.AU32259

Design and Analysis of a Helically Propelled Microswimmer

Puze Chen

Faculty of Science and Engineering, University of Nottingham Ningbo China, Ningbo, China
ssypc3@nottingham.edu.cn

Abstract. Bacteria can navigate through microscopic environments, which are highly viscous. The secret of their movement lies in the flagella on the body. These flagella spin in a spiral way in the fluid to propel the body forward. This provides the scientists an efficient strategy for propulsion under low Reynolds number. Grasping the mechanism behind is crucial for designing artificial micro swimmers. This work brings together theoretical modelling and scaled prototyping to analyse the underlying principles. First, a resistive-force-theory (RFT) model that links helical geometry to thrust was first developed. The optimal flagellar pitch angle that maximizes the speed was also obtained. The question then shifted to scalability. In reality, we can only manufacture macroscopic models. Buckingham Pi Theorem, a method of nondimensionalization, guided the scaling laws to bridge the micro to macro level. A low-cost physical model was then constructed—a plastic hull powered by a twisted rubber band driving a wire helix. The model successfully achieved forward thrust through helical rotation. Collectively, this work provides an integrated framework—combining theory and experiment—for developing bio-inspired helical propulsion systems in viscous, inertia-dominated environments.

Keywords: Helical propulsion, microswimmer, bio-inspired design

1. Flows at low Reynolds number

1.1. The basic backgrounds

Artificial micro swimmers have huge potential for biomedicine, including targeted drug delivery, minimally invasive surgery, and environmental remediation. However, downscaling a swimming machine from the human size to that of a bacterium is not simple. In our macroscopic world, a swimmer can keep moving forward after a push because inertia plays the main role. At the microscopic scale, the rule no longer applies. Viscous forces dominate to such an extent that inertia becomes negligible. This significant shift for propulsion strategy forms the central theme of this work. The locomotion in such regimes has grown into a vibrant topic in microswimmer mechanics, with applications from microbiology to robotics [1].

1.2. Typical Reynolds numbers of microswimmers and implications

The world of microorganisms is of low Reynolds numbers. For a human swimming in water, Re can be on the order of 10^4. For a small fish like a guppy, it might be 10^{-2}. However, for the bacteria and microswimmers of interest (e.g., E. coli, sperm cells), Re is typically in the range of 10^{-4} to 10^{-5} [2]. This is the realm of Stokes flow, where the Navier-Stokes equations simplify, and fluid motion

© 2026 The Authors. This is an open access article distributed under the terms of the Creative Commons Attribution License 4.0 (https://creativecommons.org/licenses/by/4.0/).

DOI: 10.54254/2753-8818/2026.AU32259

is instantaneous, reversible, and history-independent [3]. In this regime, the Reynolds number $Re = \rho UL/\mu$ becomes much less than 1, justifying the neglect of the nonlinear inertial term in the Navier-Stokes equations, leading to the linear Stokes equations [4].

An illustration by Purcell notes that if such a micro swimmer stops its propulsion, it will coast to a stop within a distance comparable to atomic dimensions in less than a microsecond [2]. Consequently, a microscopic swimmer cannot rely on momentum and must generate continuous, non-reciprocal motion to achieve net displacement. This invalidates most common macroscopic propulsion mechanisms.

1.3. The scallop theorem

A cornerstone of low-Re hydrodynamics is the "Scallop Theorem," articulated by Purcell [2]. It states that if a body deforms its shape in a reciprocal (time-symmetric) manner—meaning the sequence of shape changes during the power stroke is exactly the reverse of the recovery stroke—it will achieve zero net displacement over one complete cycle. Forward and backward motions cancel out perfectly.

The scallop, a bivalve that opens its shell slowly and closes it rapidly to jet water and move, is the archetype. At low Re, this single-hinged, one-degree-of-freedom motion is purely reciprocal and therefore completely ineffective for swimming. To achieve net motion, a swimmer must execute a non-reciprocal cycle in its configuration space. The simplest theoretical model is a "Purcell swimmer" with two hinged segments (two degrees of freedom), which can trace a loop in its configuration space to generate progressive motion [5,6].

1.4. Force and torque balance: the propulsion matrix

At low Re, the net hydrodynamic force and torque on a swimmer are linearly related to its translational velocity v and rotational velocity ω. For a simple helical propeller, like a bacterial flagellum, considering motion along its axis, this relationship can be expressed via the matrix [2,7]:

$$\begin{pmatrix} F \\ T \end{pmatrix} = \begin{pmatrix} A & B \\ B & D \end{pmatrix} \begin{pmatrix} v \\ \omega \end{pmatrix} \tag{1}$$

Here, A is the translational drag coefficient, D is the rotational drag coefficient, and the key off-diagonal coupling coefficient B represents propulsive capability. A non-zero B indicates that rotation generates thrust (force) and, conversely, that an applied force will cause rotation. The matrix is symmetric because of the reciprocal theorem in Stokes flow. For a swimmer in free motion with no external force or torque ($\mathrm{F} = 0, \mathrm{T} = 0$), this equation dictates a fixed ratio $\mathrm{v}/\omega = -\mathrm{B}/\mathrm{A}$, which defines its propulsion characteristics.

2. Model construction and numerical analysis of a helical microswimmer

2.1. Model conceptualization and governing equations

To quantitatively predict the motion of a microscale swimmer, a theoretical model is constructed. The swimmer is idealized as the object below: a spherical cell body propelled by a single rotating helical flagellum, as **Figure 1** depicted.

DOI: 10.54254/2753-8818/2026.AU32259

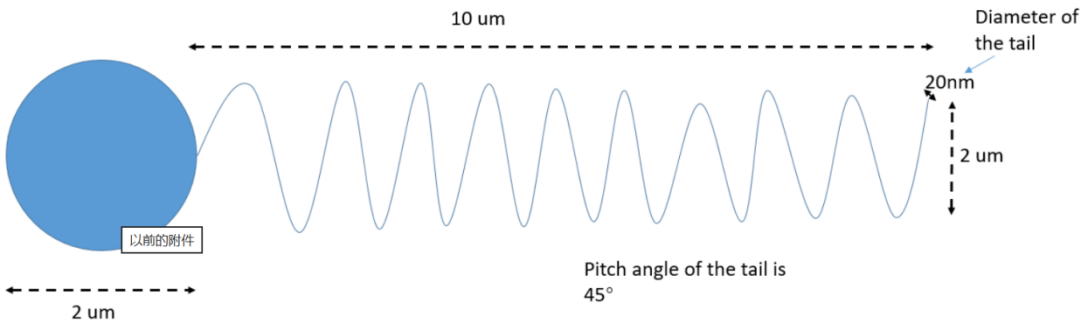


Figure 1. This is model schematic diagram

This configuration mimics E. coli.

The characteristics are governed by the following force and torque balances in Stokes flow:

$$F_c + F_f = 0 \tag{2}$$

$$T_c + T_f + T_m = 0 \tag{3}$$

where F_c, T_c are the hydrodynamic force and torque on the spherical head, F_f, T_f are those on the flagellum, and T_m is the motor torque.

For the flagellum, the linear resistance relation is expressed in matrix form as:

$$\begin{pmatrix} F_f \\ T_f \end{pmatrix} = \begin{pmatrix} \alpha_f & \gamma_f \\ \gamma_f & \beta_f \end{pmatrix} \begin{pmatrix} v \\ \omega_f \end{pmatrix} \tag{4}$$

where v is the swimming speed, ω_f is the flagellum's angular velocity, and α_f, β_f, γ_f are the translational, rotational, and coupling resistance coefficients, respectively.

For the spherical head of radius a, the resistance is isotropic [8]:

$$F_c = \alpha_c v \tag{5}$$

$$T_c = \beta_c \omega_c \tag{6}$$

with ω_c being the angular velocity of the head.

The motor torque is modeled with a linear speed-dependent characteristic:

$$T_m = T_0 \left(1 - \frac{\omega_f - \omega_c}{\omega_0}\right) \tag{7}$$

where T_0 is the stall torque, ω_0 is the zero-load speed, and $\omega_m = \omega_f - \omega_c$ is the relative motor speed.

These equations constitute a system that determines the steady-state swimming kinematics , (v, ω_f, ω_c) given the geometric parameters and motor properties.

2.2. Hydrodynamic resistance coefficients

The accuracy of the model depends on the correct calculation of the resistance coefficients $\alpha_c, \beta_c, \alpha_f, \beta_f, \gamma_f$.

For a sphere of radius a in a Newtonian fluid of viscosity μ, the classic Stokes laws give:

$$\alpha_c = -6\pi\mu a \tag{8}$$

$$\beta_c = -8\pi\mu a^3 \tag{9}$$

The negative signs indicate that the force and torque oppose the motion.

DOI: 10.54254/2753-8818/2026.AU32259

For a long, thin helix with length L, filament diameter d, helix radius r, and pitch $p = 2\pi r/\tan\theta$ (where θ is the pitch angle), the integrated coefficients are given by:

$$\alpha_f = \frac{2\pi\mu L}{\Lambda(4\pi^2r^2+p^2)}(8\pi^2r^2 + p^2) \tag{10}$$

$$\beta_f = \frac{2\pi\mu L}{\Lambda(4\pi^2r^2+p^2)}(4\pi^2r^2 + 2p^2)r^2 \tag{11}$$

$$\gamma_f = \frac{2\pi\mu L}{\Lambda(4\pi^2r^2+p^2)}(-2\pi r^2 p) \tag{12}$$

where $\Lambda = \log(d/2p) + 0.5$ is a logarithmic factor arising from the slenderness of the filament.

The system of equations forms a closed set of linear equations with the unknowns v, ω_f, and ω_c. Following the algebra presented by Magariyama and Kudo, the swimming speed can be solved as:

$$v = K_0\beta_c\gamma_f, \text{with} K_0 = \left[\frac{\beta_c(\alpha_c\beta_f+\alpha_f\beta_f-\gamma_f^2)}{T_0} - \frac{\alpha_c\beta_c+\alpha_c\beta_f+\alpha_f\beta_c+\alpha_f\beta_f-\gamma_f^2}{\omega_0}\right]^{-1} \tag{14}$$

We implemented this model in MATLAB (see Appendix A for the code structure) to solve the specific problem.

2.3. Results

The steady-state kinematics are: $v = 1.543 \times 10^{-5}$ m/s, $\omega_f = 1.013 \times 10^2$ rad/s($\approx$ 16.1 Hz), $\omega_c = -6.067 \times 10^1$ rad/s.

The negative sign of ω_c confirms the counter-rotation of the cell body due to torque balance, a well-known phenomenon in bacterial motion. The predicted swimming speed is within the characteristic range of flagellated bacteria (e.g., E. coli ~20–30 μm/s), considering the smaller head size and specific motor parameters used here. The result validates that a rotating helical filament in a viscous fluid generates directional thrust through the coupling coefficient γ_f.

The ratio $v/(2\pi\omega_f) \approx 2.43$ nm per revolution indicates the distance advanced per full turn of the helix, serving as a measure of propulsive efficiency at low Re. The small value underscores the highly resistive environment. This model offers a workable framework for designing artificial microswimmers. Researchers can adjust geometric parameters—helical radius, pitch angle, filament length—and motor traits to further optimize swimming speed and energy efficiency.

2.4. Improvements of the code

The geometry of the helical propeller is a critical design parameter for microswimmers. To systematically investigate its impact, we performed a parameter sweep on the pitch angle θ, while holding all other parameters (head size, flagellum length, motor properties, etc.) constant. The code structure can be found in Appendix B.

The result is shown in **Figure 2**.

DOI: 10.54254/2753-8818/2026.AU32259

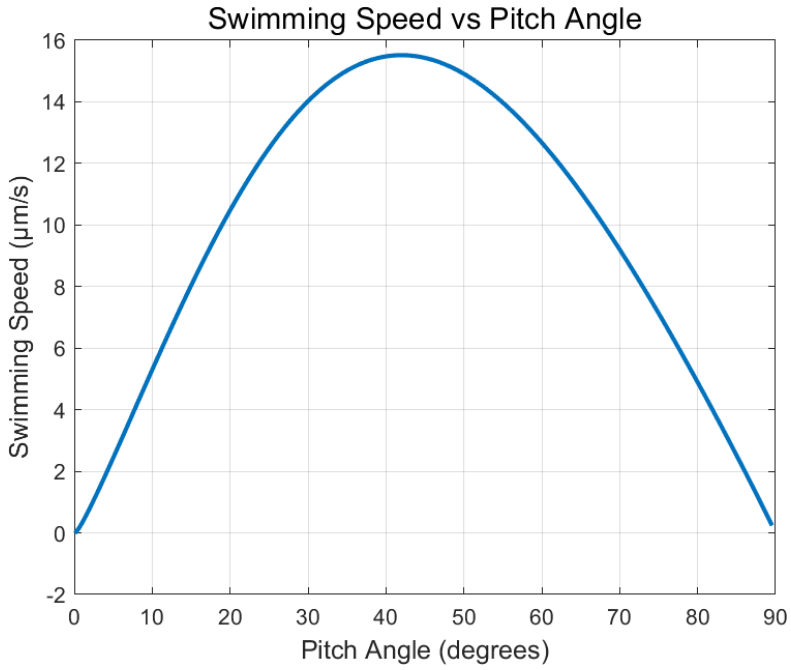


Figure 2. This is the swimming speed as a function of pitch angle

The graph reveals an optimal pitch angle that maximizes propulsion speed.

In low pitch angles ($\theta \to 0°$), the helix is tightly wound, leading to excessive drag along the swimming axis. Despite some propulsive coupling, net thrust is negligible. In the optimal region ($\theta_{opt} \approx 40°–50°$), the swimming speed peaks as the helical geometry achieves an ideal balance between thrust generation and drag resistance. Lastly, the helix approaches a straight rod in high pitch angles ($\theta \to 90°$), eliminating the helical asymmetry needed for directional thrust. Propulsive coupling vanishes, resulting in no speed.

3. Dimensional analysis: bridging microscopic principles to macroscopic design

3.1. Dimensional analysis and the buckingham Pi theorem

The preceding numerical model predicts the performance of a model. However, engineering design and experimental prototyping often require understanding how to correctly translate from a macro-scale test rig to a microscopic robot [9]. Dimensional analysis and the Buckingham Pi Theorem provide the fundamental framework for this purpose [10,11].

The theorem states that if a physical process involving n dimensional variables is dimensionally homogeneous (i.e., all terms in its governing equations have consistent dimensions), it can be described by a relationship among $r = n - m$ independent dimensionless Pi terms (Π), where m is the number of fundamental dimensions (e.g., Mass M, Length L, Time T) involved. This leads to a profound simplification:

$$F(A_1, A_2, \ldots, A_n) = 0 \to f(\Pi_1, \Pi_2, \ldots, \Pi_r) = 0 \tag{14}$$

where A_i are the dimensional variables and Π_i are dimensionless groups.

3.2. Derivation of key dimensionless parameters for microswimming

We can now systematically derive the governing dimensionless groups for low-Reynolds-number propulsion.

DOI: 10.54254/2753-8818/2026.AU32259

Consider the drag force F_D on a body of characteristic length L moving at velocity V in a fluid of density ρ and viscosity μ. The functional relationship is:

$$F_D = f(L, V, \rho, \mu) \tag{15}$$

Performing dimensional analysis (as detailed in the problem solution) yields two Pi terms:

$$\Pi_1 = \frac{F_D}{\rho V^2 L^2} \tag{16}$$

$$\Pi_2 = \frac{\mu}{\rho V L} = Re^{-1} \tag{17}$$

Thus, the relationship simplifies to:

$$\frac{F_D}{\rho V^2 L^2} = f(Re), \text{ or, } C_D = f(Re) \tag{18}$$

where $C_D = F_D/(\frac{1}{2}\rho V^2 A)$ is the drag coefficient. This confirms that for geometrically similar bodies, the drag coefficient depends solely on the Reynolds number.

3.3. Implications for microswimmers design

To study the micro swimmer in a lab setting, one could build a scaled-up model operating in a high-viscosity fluid. For dynamic similarity, the model must match the key Pi terms of the microswimmer, primarily a very low Reynolds number ($Re \ll 1$). This might involve using a large model in a very viscous fluid like corn syrup, ensuring that inertial forces remain negligible relative to viscous forces.

Dimensional analysis suggests how swimmer performance varies with size. When all geometric dimensions are reduced by a factor k ($L \to L/k$), and the motor torque scales down by the volume of the motor ($T_0 \propto L^3 \to T_0/k^3$), the swimming speed v would scale approximately as $v \propto L$ to maintain constant stress and similar Pi terms. The findings provide important guidance for miniaturization.

In complex (non-Newtonian) biological fluids, however, additional dimensionless groups (e.g., the Deborah number, comparing fluid relaxation time to swimmer time scale) might also affect outcomes, necessitating more sophisticated similitude criteria [12,13].

4. Low-cost, rubber-powered scaled model

To examine the principles of helical propulsion under limited experimental conditions, we designed and constructed a simplified macroscopic model driven by elastic energy stored in the spring. This hands-on approach provides an intuitive demonstration of the propulsion mechanism without requiring complex micro-motors.

The hull is a hollow plastic cylinder, shaped like a streamlined torpedo. A cone at the front reduces drag; the rear remains open to accommodate the drive mechanism. A stainless steel wire is coiled into a helix, its geometry scales from the bacterial flagellum model in Section 2. This helix is anchored to a plastic disc that rotates freely at the stern, held in place only by the tension of the rubber band.

The power source is a single rubber band, slightly shorter than the hull. One end hooks inside the nose cone; the other attaches to the tail rotor disc. Before each trial, the disc need to be manually twisted—typically 50 to 100 revolutions. This action twists the rubber band, storing elastic potential energy [14]. The wound assembly is then kept locked to prevent unwinding before submersion.

Upon immersion and release, the unwinding rubber band applies torque. This drives the helical tail to rotate relative to the surrounding water, generating forward thrust.

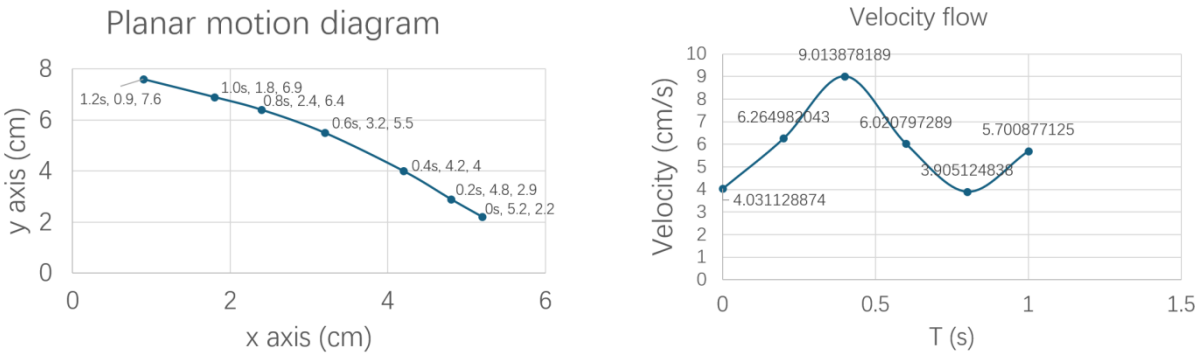
The final assembly schematic is shown in **Figure 3**.

DOI: 10.54254/2753-8818/2026.AU32259



Figure 3. This is the fabricated prototype used in experiments

The model's motion is recorded with a camera and calibrated with a scale bar. The video is then analyzed using motion-tracking software to extract the nose displacement x(t), shown in **Figure 4**, from which the steady-state swimming speed v is calculated as the average velocity during the propulsion phase.



(a) This is the trajectory diagram

(b) This is the velocity-time plot

Figure 4. These are the motion diagram

The steady-state speed recorded in water was 5.83 cm/s, which can be scaled up to predict the corresponding velocity at microscopic level.

5. Conclusion

In this research, a RFT model was established for the microswimmers propelled by helical flagella. After the motion system was developed, a pitch angle sweep revealed that the optimal angle for the helix lies between 40°–50°. Buckingham Pi theorem identified the Reynolds number as the key parametre that governs dynamic similarity. This framework allowed microscopic design principles to be translated to a macroscopic scale. Guided by these scaling laws, a low-cost demonstrator was constructed—a plastic hull powered by a twisted rubber band driving a wire helix. When submerged, the model achieved a speed of 5.83 cm/s, within the rational range. Discrepancies could be traced to friction in the rotating joint, energy dissipation in the rubber band, and non-ideal helix geometry. The findings lead to some conclusions. First, the governing principles can hold across different size scales, as long as the key dimensionless groups are kept the same. Second, the equations listed and optimal pitch angle found above gave a useful starting point for designing artificial microswimmers. Third, the macroscopic prototype offers a simple way to test design ideas before microfabrication—by changing key parameters and checking if the predictions still hold.

Looking ahead, the findings have huge potential in the biomedical field. A microfabricated swimmer, if realized, could apply surface modifications for auto-navigation, therefore traverse biological barriers that are unreachable by conventional methods, and integrate sensors for pH or

DOI: 10.54254/2753-8818/2026.AU32259

enzyme-triggered drug release. With external magnetic field or ultrasonic guidance, such devices could achieve adaptive path planning and on-demand activation, therefore transform such devices into tools for personalized precise medicine delivery [15].

References

[1] Bechinger, C., et al. (2016). Active particles in complex and crowded environments. Reviews of Modern Physics, 88(4), 045006. https://doi.org/10.1103/RevModPhys.88.045006

[2] Purcell, E. M. (1977). Life at low Reynolds number. American Journal of Physics, 45(1), 3–11. https://doi.org/10.1119/1.10903

[3] Lauga, E., & Powers, T. R. (2009). The hydrodynamics of swimming microorganisms. Reports on Progress in Physics, 72(9), 096601. https://doi.org/10.1088/0034-4885/72/9/096601

[4] Happel, J., & Brenner, H. (2012). Low Reynolds number hydrodynamics: with special applications to particulate media. Springer Science & Business Media.

[5] Lauga, E. (2016). Bacterial hydrodynamics. Annual Review of Fluid Mechanics, 48, 105-130. https://doi.org/10.1146/annurev-fluid-122414-034606

[6] Zhang, L., et al. (2009). Artificial bacterial flagella: Fabrication and magnetic control. Applied Physics Letters, 94(6), 064107. https://doi.org/10.1063/1.3079655

[7] Brennen, C., & Winet, H. (1977). Fluid mechanics of propulsion by cilia and flagella. Annual Review of Fluid Mechanics, 9(1), 339-398. https://doi.org/10.1146/annurev.fl.09.010177.002011

[8] Magariyama, Y., & Kudo, S. (2002). A mathematical explanation of an increase in bacterial swimming speed with viscosity in linear-polymer solutions. Biophysical Journal, 83(2), 733–739. https://doi.org/10.1016/S0006-3495(02)75204-1

[9] Kim, M., Bird, J. C., Van Parys, A. J., Breuer, K. S., & Powers, T. R. (2003). A macroscopic scale model of bacterial flagellar bundling. Proceedings of the National Academy of Sciences of the United States of America, 100(26), 15481-15485. https://doi.org/10.1073/pnas.2633596100

[10] Evans, J. H. (1972). Dimensional Analysis and the Buckingham Pi Theorem. American Journal of Physics, 40(12), 1815-1822. https://doi.org/10.1119/1.1987069

[11] Ciulla, G., D'Amico, A., & Lo Brano, V. (2017). Evaluation of building heating loads with dimensional analysis: Application of the Buckingham π theorem. Energy and Buildings, 154, 479-490. https://doi.org/10.1016/j.enbuild.2017.08.043

[12] Lauga, E. (2007). Propulsion in a viscoelastic fluid. Physics of Fluids, 19, 083104. https://doi.org/10.1063/1.2751388

[13] Elfring, G., & Lauga, E. (2015). Theory of locomotion through complex fluids. In S. E. Spagnolie (Ed.), Complex fluids in biological systems. https://doi.org/10.48550/arXiv.1410.4322

[14] Olson, S. D., Lim, S., & Cortez, R. (2013). Modeling the dynamics of an elastic rod with intrinsic curvature and twist using a regularized Stokes formulation. Journal of Computational Physics, 238, 169-187. https://doi.org/10.1016/j.jcp.2012.12.026

[15] Nelson, B. J., Kaliakatsos, I. K., & Abbott, J. J. (2010). Microrobots for minimally invasive medicine. Annual Review of Biomedical Engineering, 12, 55-85. https://doi.org/10.1146/annurev-bioeng-010510-103409

Appendix A

```
clc

clear

%% Parameters (SI)
mu    = 0.89e-3;      % Dynamic viscosity of water
L     = 10e-6;        % Flagellum length (m)
```

DOI: 10.54254/2753-8818/2026.AU32259

```
d     = 20e-9;          % Flagellum diameter (m)
r     = 1e-6;           % Helix radius (m)
theta = 45;             % Helix pitch angles (deg)

a     = 1.0e-6;         % Cell body half-width (the radius of the head)
b     = 1e-6;           % Cell body half-length (ditto)

T0    = 1.5e-18;        % Stall torque
w0    = 1700;           % Zero-torque motor speed (rps)

%% Step-1 : Calculate the pitch p
p = 2*pi*r*tand(theta);           % Pitch

%% Step-2 : Find the drag coefficients α_f β_f γ_f for the tail
denom_f = (log(d/(2*p)) + 0.5) * (4*pi^2*r^2 + p^2);  % Shared denom.
term    = 2 * pi * mu * L;        % Shared term in the numerator

alpha_f = (8 * pi^2 * r^2 + p^2) * term / denom_f;
beta_f  = (4 * pi^2 * r^2 + 2 * p^2)*r^2 * term / denom_f;
gamma_f = (-2 * pi * r^2 * p) * term / denom_f;

%% Step-3 : Cell-body coefficients α_c β_c
```

DOI: 10.54254/2753-8818/2026.AU32259

```
%  μ_N* = μ_T* = μ because swimmer is in water.
alpha_c = -6 * pi * mu * a * (1 - (1/5)*(1 - b/a));
beta_c  = -8 * pi * mu * a^3 * (1 - (3/5)*(1 - b/a));

%% Step-4 : Find K0
term1 =  beta_c * (alpha_c*beta_f + alpha_f*beta_f - gamma_f^2) / T0;
term2 = (alpha_c*beta_c + alpha_c*beta_f + alpha_f*beta_c + alpha_f*beta_f - gamma_f^2) / w0;

K0 = 1 / ( term1 - term2 );

%% Final solution
% Swimming speed ν
v = K0 * beta_c * gamma_f;
% Flagella rotational speed ω_f
omega_f = -K0 * (alpha_c*beta_c + alpha_f*beta_c);
% Cell-body rotational speed ω_c
omega_c =  K0 * (alpha_c*beta_f + alpha_f*beta_f - gamma_f^2);

%% Display results
fprintf('Flagellum drag : alpha_f = %.3e   beta_f = %.3e   gamma_f = %.3e  (N·s/m)\n', alpha_f, beta_f, gamma_f);

fprintf('Cell body drag : alpha_c = %.3e   beta_c = %.3e  (N·s/m)\n', alpha_c, beta_c);
```

DOI: 10.54254/2753-8818/2026.AU32259

```
51
52 fprintf('Swimming speed ν = %.3e (m/s)\n', v);
53 fprintf('Flagellum ω_f = %.3e 1/s\n', omega_f);
54 fprintf('Cell body ω_c = %.3e 1/s\n', omega_c);
55
56 clc
57 clear
```

Appendix B

```
1  clc;
2  clear;
3
4  %% Parameters (SI)
5  mu = 0.89e-3;    % Dynamic viscosity of water
6  L = 10e-6;        % Flagellum length (m)
7  d = 20e-9;        % Flagellum diameter (m)
8  r = 1e-6;         % Helix radius (m)
9  a = 1e-6;         % Cell body half-width (the
   radius of the head here)
10 b = 1e-6;         % Cell body half-length (ditto)
11 T0 = 1.5e-18;     % Stall torque
12 w0 = 1700;        % Zero-torque motor speed (rps)
13
14 %% Vary the pitch angle from 0 to pi/2
15 theta_range = linspace(0.1, 90, 200);    % Here we
   must avoid exactly 0 to prevent tan(0)
16 v_range = zeros(size(theta_range));       %
   Swimming speed storage
```

DOI: 10.54254/2753-8818/2026.AU32259

```
17
18 for i = 1:length(theta_range)
19     theta = theta_range(i);
20     p = 2 * pi * r * tand(theta);          % Pitch
21
22     % Step-2: Drag coefficients of tail
23     denom_f = (log(d / (2 * p)) + 0.5) * (4 * pi^2
   * r^2 + p^2);
24     term = 2 * pi * mu * L;
25     alpha_f = (8 * pi^2 * r^2 + p^2) * term /
   denom_f;
26     beta_f  = (4 * pi^2 * r^2 + 2 * p^2) * r^2 *
   term / denom_f;
27     gamma_f = (-2 * pi * r^2 * p) * term /
   denom_f;
28
29     % Step-3: Drag coefficients of cell body
30     alpha_c = -6 * pi * mu * a * (1 - (1/5)*(1 -
   b/a));
31     beta_c  = -8 * pi * mu * a^3 * (1 - (3/5)*(1 -
   b/a));
32
33     % Step-4: Compute K0
34     term1 = beta_c * (alpha_c * beta_f + alpha_f *
   beta_f - gamma_f^2) / T0;
35     term2 = (alpha_c * beta_c + alpha_c * beta_f +
   alpha_f * beta_c + alpha_f * beta_f - gamma_f^2) /
   w0;
36     K0 = 1 / (term1 - term2);
37
```

DOI: 10.54254/2753-8818/2026.AU32259

```
38      % Step-5: Swimming speed
39      v = K0 * beta_c * gamma_f;
40      v_range(i) = v;
41  end
42
43  %% Plotting
44  figure;
45  plot(theta_range, v_range * 1e6, 'LineWidth',
    2);  % Convert m/s to μm/s
46  xlabel('Pitch Angle (degrees)', 'FontSize', 12);
47  ylabel('Swimming Speed (μm/s)', 'FontSize', 12);
48  title('Swimming Speed vs Pitch Angle', 'FontSize',
    14);
49  grid on;
```